From electron crystallography to single particle cryoEM

Nobel Lecture, December 8, 2017 by
Richard Henderson
MRC Laboratory of Molecular Biology, Cambridge, U.K.

INTRODUCTION AND BACKGROUND IN X-RAY CRYSTALLOGRAPHY

After completing an undergraduate physics degree at Edinburgh University in 1966, and deciding to pursue Ph.D. research in biophysics, I had the good fortune to consult Professor Bill Cochran who suggested I write to Max Perutz, at that time head of the recently opened Medical Research Council Laboratory of Molecular Biology (MRC-LMB) in Cambridge. Perutz offered me a 3-year MRC Scholarship to work with David Blow on the proteolytic enzyme chymotrypsin. I arrived just as the chymotrypsin group was calculating a 3-dimensional (3D) Fourier map using two heavy-atom derivatives for phasing. Unfortunately, that first map was only partly interpretable, with electron density for only 10 of the 241 amino-acid residues recognisable, and since Brian Matthews was just leaving for a new postdoctoral position at the NIH, I was invited to join the "chymotrypsin team", in which Paul Sigler was the only other scientist, to help determine the structure. After about 6 months' work collecting data for a third heavy-atom derivative, the next 3D Fourier map proved to be fully interpretable, so I found myself soon after my arrival in Cambridge transformed into a trained X-ray crystallographer and co-author of a paper (Matthews et al, 1967) describing the 3D structure of chymotrypsin. At the end of that first year, I then embarked on my thesis research into sub-

strate and inhibitor binding to chymotrypsin, working initially alongside and then in collaboration with Tom Steitz, who had arrived as a postdoctoral fellow that summer. By 1969 we had obtained a number of informative 3D difference Fourier maps that allowed us to understand substrate and inhibitor binding to chymotrypsin and to explain the hydrolytic mechanism (Steitz et al, 1969; Henderson, 1970).

My transition from X-ray crystallographer to electron crystallographer followed indirectly from my postdoctoral experiences at Yale, where I had decided to work on membrane protein structure and had tried to tackle voltage-gated sodium channels (VGSCs) from garfish olfactory nerves. I had found that the VGSCs, assayed by a tritiated-tetrodotoxin ligand-binding assay were unstable after solubilisation in detergent (Henderson & Wang, 1972), so had switched to working on the small, stable and abundant membrane protein bacteriorhodopsin that had been discovered by Walther Stoeckenius and his collaborators in the purple membrane fraction from *H. halobium* (Oesterhelt & Stoeckenius, 1971; Blaurock & Stoeckenius, 1971).

BACTERIORHODOPSIN AT 7 Å, THEN 3.5 Å, REFINEMENT & KINETICS

Following my return to the MRC-LMB, I gave a talk in the annual laboratory symposium in October 1973 about my ideas for trying to solve the structure of bacteriorhodopsin. Since bacteriorhodopsin had been shown (Blaurock & Stoeckenius, 1971) to consist of well-ordered two-dimensional (2D) crystals in the membranes of *H. halobium*, I had two ideas. One was to use X-ray powder diffraction of these native membranes with multiple heavy atom derivatives to phase and resolve the problem of overlapping reflections. The other was to make 3D crystals from detergent-solubilised monomeric bacteriorhodopsin. Neither of these ideas worked out, but in the same symposium I heard an impressive talk by Nigel Unwin about his work to record high-quality electron microscope images of negatively stained tobacco mosaic virus (TMV) using a phase plate that he had constructed from a single thread of spider web silk coated with gold. Afterwards, we discussed the possibility of recording images and electron diffraction patterns from 2D crystals of bacteriorhodopsin without using negative stain. A very productive 18-month collaboration ensued, culminating in the determination of the 7 Å 3D structure of bacteriorhodopsin (Unwin & Henderson, 1975; Henderson & Unwin, 1975), shown in Figure 1 & Figure 2, determined using electron diffraction and electron microscopy of 2D crystals of bacteriorhodopsin at room temperature embedded in a thin film of glucose. Nigel and I wondered why this electron crystallographic method had produced a 3D density

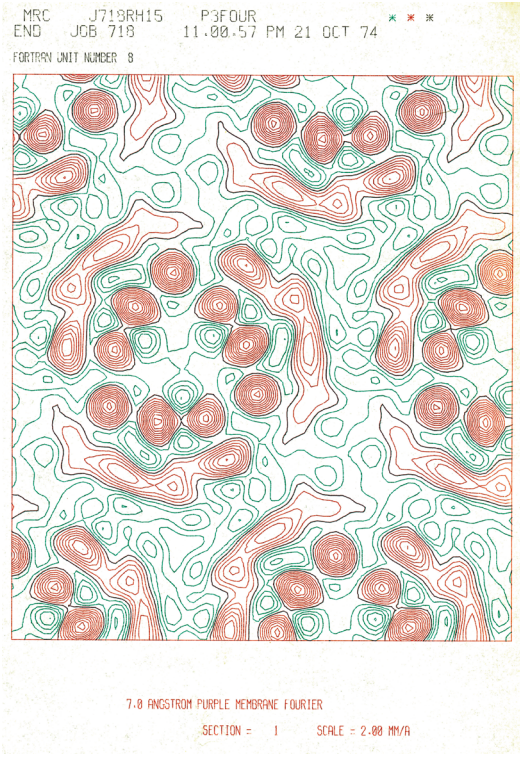

Figure 1. The first projection structure at 7 Å resolution of the purple membrane calculated in October 1974 using 36 reflections obtained by room-temperature electron diffraction and imaging of glucose-embedded 2D crystals of bacteriorhodopsin (Unwin & Henderson, 1975).

map at only 7 Å resolution, when there was nothing about the approach that intrinsically limited the resolution. We thought that the recording of images on film might be a limiting factor and spent time investigating different photographic emulsions. We also thought that the film scanners that were available in the 1970s for digitising the images might be degrading the information and spent time building and improving film scanners. This produced only fairly small improvements.

At that stage, having come into structural biology through X-ray diffraction in which all the phases of the Fourier components, as observed through Bragg diffraction from the crystal lattice, had to be determined indirectly, I also thought that electron diffraction was intrinsically more promising than electron microscopy because the elegant simplicity of recording electron diffraction patterns compared favourably with the multiple difficulties of recording good images. We therefore spent several years trying to extend the resolution of the bacteriorhodopsin structure using a number of diffraction-based approaches. Figure 3 summarises the different ideas we tried. Tom Ceska tried to make heavy atom derivatives (Ceska & Henderson, 1990). Joyce Baldwin and Michael Rossmann tried molecular replacement (Tsygannik & Baldwin, 1987; Rossmann & Hender-

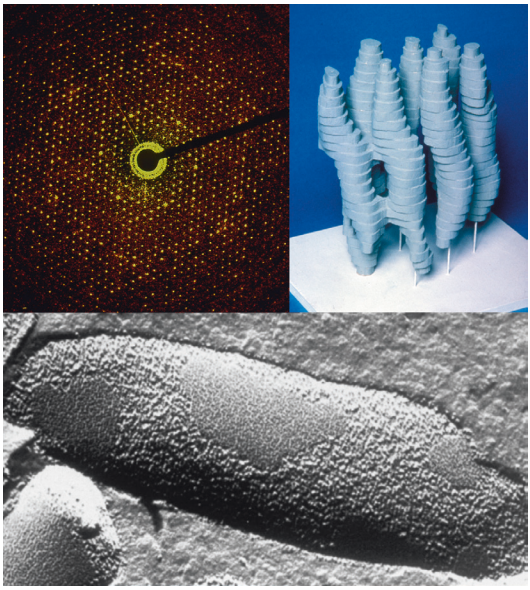

Figure 2. The structure of bacteriorhodopsin at 7 Å resolution in 3D from 18 images and 15 diffraction patterns. The collage shows (a) freeze-fracture picture from Walther Stoeckenius, (b) electron diffraction pattern obtained much later using a phosphor/fibre-optics/CCD camera, (c) the 1975 balsawood model of a single bacteriorhodopsin molecule (Henderson & Unwin, 1975).

son, 1982). David Agard tried to extend the phases using a multi-parameter model building approach (unpublished). Although all of these approaches gave hints of success that were encouraging at times, none of them were powerful enough to give phases that resulted in convincing maps that were interpretable much beyond the resolution obtained in 1975. It was not until Tzyy-Wen Jeng and Wah Chiu demonstrated, in a collaboration with Fritz Zemlin (Jeng et al, 1984), that images showing clearly visible diffraction spots at 3.9 Å resolution could be obtained from thin 3D crystals of rattlesnake venom crotoxin using an electron microscope in Berlin with a liquid-helium superconducting objective lens, that I became convinced electron cryomicroscopy could produce high quality images. We therefore embarked, as a last resort, on using electron cryomicroscopy for high-resolution phase determination (see Figure 4). In earlier years, Bob Glaeser's group had shown that freezing thin 3D crystals of catalase could produce good electron diffraction patterns and images (Taylor & Glaeser, 1974; 1976) and that there was a benefit in terms of reduced radiation damage (Glaeser, 1971), but I had been unconvinced by earlier attempts to show that electron cryomicroscope images of purple membrane contained high-resolution information (Hayward & Stroud, 1981).

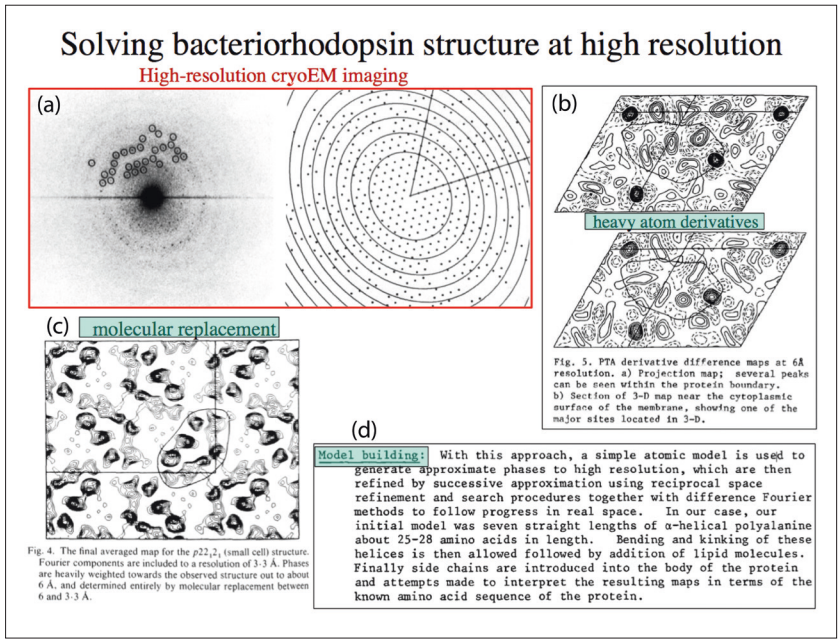

Figure 3. Overview of methods used in the early 1980s to try to solve the structure of bacteriorhodopsin at high resolution. (a) an optical diffraction pattern of a high-resolution projection image from the cryomicroscope in Berlin with the detectable spots encircled alongside the computed transform with the same Fourier components that were detected after computer processing from Henderson et al (1986). (b) difference Fourier maps of a heavy atom derivative, in this case phosphotungstate (PTA) from Ceska & Henderson (1990). (c) result of an attempt to extend the phases by molecular average and phase refinement from Rossmann & Henderson (1982). (d) attempts to bootstrap the phases to high resolution by using a model consisting of a bundle of 7 α-helices, from unpublished work by David Agard. Although each method did produce improvements in the 3D maps, only method (a) was powerful enough to solve the high-resolution structure.

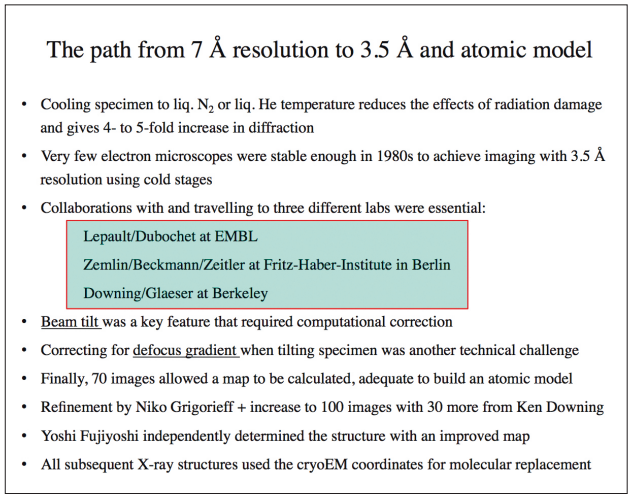

Figure 4. Summary of the key steps in the path from 7 Å to 3.5 Å resolution.

The change of emphasis from diffraction to imaging proved to be very challenging. I began with a visit to Jacques Dubochet's laboratory at the European Molecular Biology Laboratory (EMBL) in Heidelberg in 1984, working with Jean Lepault to record images on their hybrid Zeiss/Siemens microscope with the same design of superconducting liquid-helium objective lens as on the Berlin microscope. We spent a week with that home-constructed microscope, which turned out to be very unreliable. Fortunately, we managed to obtain just one image that showed diffraction beyond 4 Å resolution, although because of the difficulty of alignment and the short mean time between failures, that image had over 5000 Å of astigmatism. We did not pursue further imaging at EMBL. Nevertheless, that was the first image that allowed us to begin developing procedures for the computer-based processing of high-resolution images from 2D crystals of unstained membrane proteins. After my visit to EMBL Heidelberg, Elmar Zeitler invited me to the Fritz-Haber Institute of the Max-Planck-Society in Berlin where the superconducting lens was installed on an old Siemens 100 keV electron microscope with a conventional tungsten electron source. My first visit to Berlin, which initiated a decade-long collaboration with Fritz Zemlin and Erich Beckmann, proved even less productive than the visit to EMBL. No good images were obtained at all, but Fritz Zemlin was able to use the problems we encountered as justification to initiate a programme of improvements in the reliability of the microscope, which they called Suleika, so that by 1986, we had obtained a reasonable number of high resolution images of bacteriorhodopsin in projection. Finally, during his sabbatical visit to MRC-LMB in 1984, Bob Glaeser had suggested that Ken Downing should record some cryoEM images from purple membranes on their JEOL 100B at Berkeley. As a result, we also had an image from Ken Downing on a third electron cryomicroscope that also showed diffraction beyond 4 Å resolution.

After extensive computer processing of these early "high-resolution" projection images of 2D crystals of bacteriorhodopsin, the diffraction peaks at and beyond 4 Å resolution were clearly visible well above the noise level, just as they had been on Wah Chiu's crotoxin images two years earlier, yet when we looked for consistency, the phases from different images were in total disagreement. The phases were essentially random numbers beyond about 6 Å resolution. In the end, the explanation was that we were not taking into consideration the beam tilt arising from inaccurate alignment of the illumination along the optical axis of the microscope. By reading the literature, especially publications in *Ultramicroscopy*, I found two papers. One was entitled "The importance of beam alignment ... in high resolution electron microscopy" (Smith et al, 1983). The other was by our collaborator Fritz Zemlin! (Zemlin, 1979). Both

explained how beam-tilt misalignment perturbed the high-resolution phases with an error that was proportional to the cubed power of resolution. As soon as a beam-tilt correction factor, consisting of two extra parameters, was added to our computer programs, all the observations immediately clicked into perfect agreement and we were able to publish a comprehensive paper (Henderson et al, 1986) describing the projection structure of bacteriorhodopsin at 3.5 Å resolution, which in passing showed that previous efforts at determination of the projection structure, including our own, had all been incorrect. The final hurdle was to develop a method to correct for the gradient of defocus due to the height difference across images of tilted and highly tilted specimens, which was needed to extend the method into three dimensions. We called this the tilt-transfer function (TTF) correction (Henderson & Baldwin, 1986). It also proved much harder to obtain high quality images from tilted specimens than from untilted specimens because beam-induced charging and physical motion caused image blurring and thus greater loss of information in the vertical direction than in the plane parallel to membranes. This beam-induced image blurring problem on highly tilted specimens was helped by spotscan imaging (Bullough & Henderson, 1987; Downing 1988), especially when coupled with the improved coherence from the field emission source on the Berkeley JEOL microscope. In parallel with visits to and collaborations with Berlin and Berkeley, we also tried to develop a better side-entry cold stage at MRC-LMB in Cambridge (Henderson et al, 1991), so the eventual high-resolution 3D map of bacteriorhodopsin (Henderson et al, 1990), which allowed us to build an atomic model for most of the amino acids in the structure (Figure 5), contained a small number of images from Cambridge that supplemented the bulk of the data from Berlin and Berkeley.

Later on, Werner Kühlbrandt used the same methods, in collaboration with Yoshi Fujiyoshi, to determine the structure of the light-harvesting complex LHC-II from green plants (Kühlbrandt et al, 1994), and Ken Downing, Eva Nogales and Sharon Wolf determined the atomic structure of the αβ-tubulin dimer from 2D "zinc sheet" crystals (Nogales et al, 1998). The difficulties and limitations encountered during the bacteriorhodopsin work made it clear that the development of cryoEM would need substantial improvements in the microscope technology, especially more stable cold stages, higher vacuums, and brighter field emission sources. Also, at that time we thought higher acceleration voltage was needed to improve the electron optics of the column. These improvements were all developed slowly over the next 10 years, laying the foundations for other types of cryoEM including work with single particles.

After the 1990 publication describing the first atomic model of bacteriorhodopsin, we worked on trapping the intermediates in the light-driven

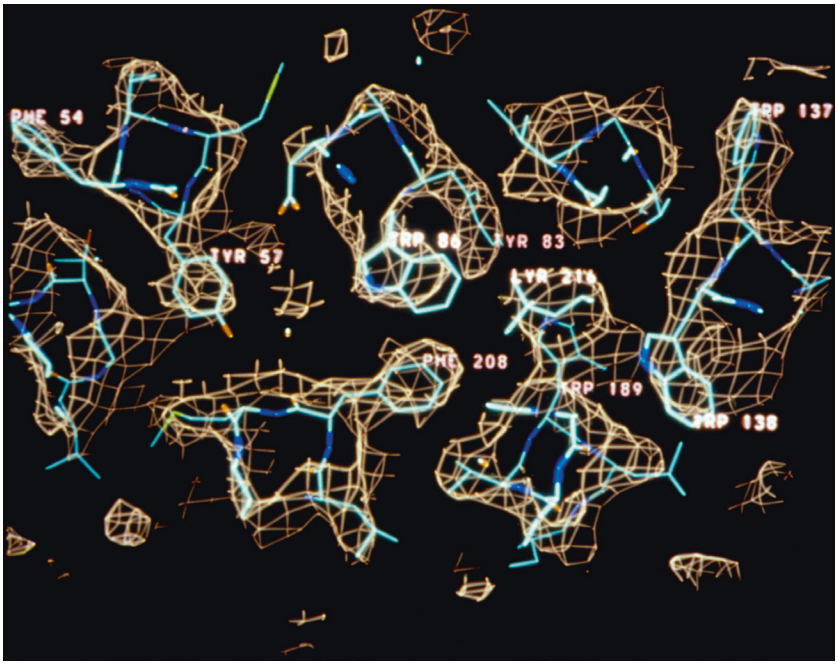

Figure 5. A slice through the central region of the 3.5 Å resolution 3D map with the corresponding atomic model superimposed, showing side chains of phenylalanine, tyrosine and tryptophan residues as well as part of the β-ionone of the chromophore retinal, which was the highest density feature in the map, from Henderson et al (1990).

photocycle (Subramaniam et al, 1993; 1999; Subramaniam & Henderson, 2000) and on the crystallographic refinement of the atomic model after the addition of a few more images from tilted specimens (Grigorieff et al, 1996). Although our work had come to its natural conclusion, the structure of bacteriorhodopsin continued to be improved both by electron microscopy (Kimura et al, 1997) and by X-ray crystallography once 3D crystals that diffracted well without twinning were obtained (PebayPeyroula et al, 1997; Lücke et al, 1999). There are now well over 100 sets of bacteriorhodopsin coordinates deposited in the Protein Data Bank (PDB).

DUBOCHET PLUNGE-FREEZE METHOD

In 1978, John Kendrew persuaded Jacques Dubochet to join the EMBL in Heidelberg to develop electron cryomicroscopy and to investigate the properties of frozen water with the goal of the determination of biological structures using cryoEM. In a series of seminal papers in the early 1980s, Dubochet and his colleagues worked out the conditions necessary to produce hexagonal ice, cubic ice and amorphous ice and how to interconvert them (Dubochet et al, 1982a; 1982b; 1984). This led to the development of their

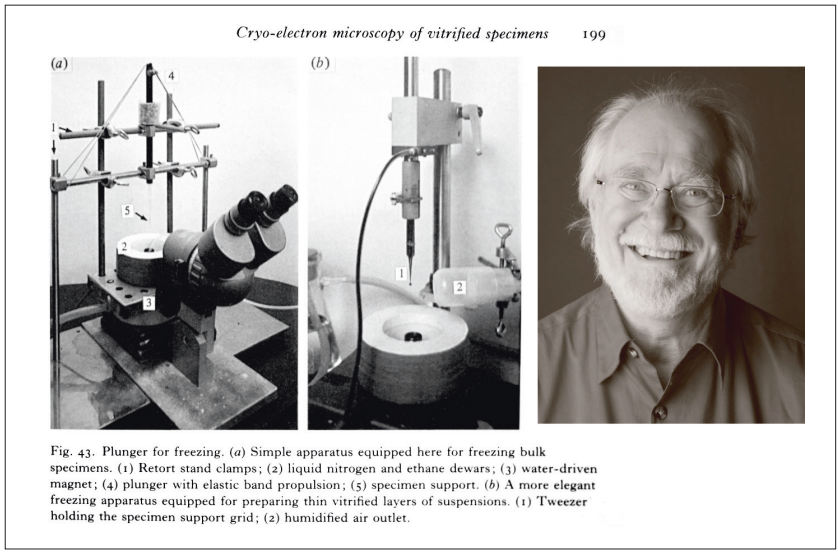

Figure 6. Early apparatus developed for plunge-freezing by the group of Jacques Dubochet at EMBL, from Dubochet et al (1988). A recent photograph of Dubochet is also shown.

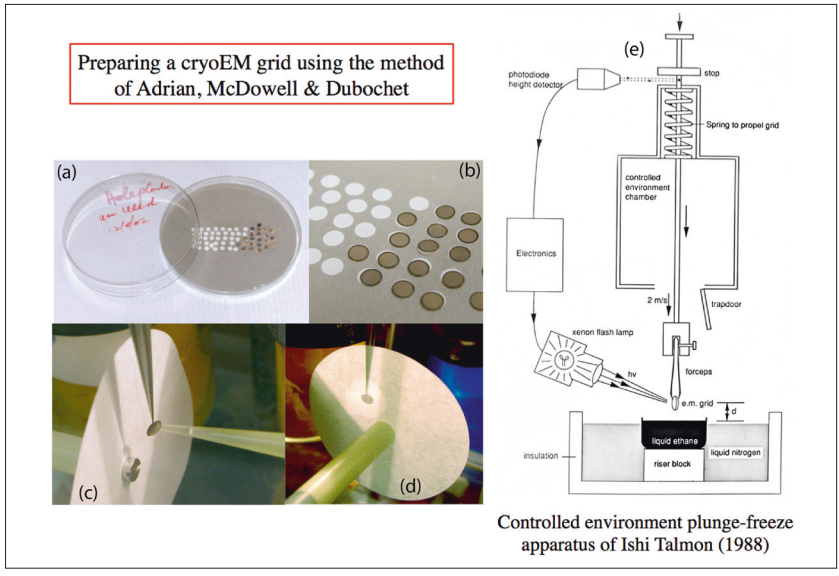

Figure 7. A series of photographs and a diagram to illustrate the plunge-freeze method of Dubochet. (a) Petri dish with about 60 grids coated with holey carbon made by Claudio Villa at MRC-LMB in 2002. (b) at higher magnification. (c) single grid to which a 3ml droplet is being applied. (d) blotting procedure. (e) schematic diagram of the plunge-freeze apparatus we used for trapping bacteriorhodopsin intermediates in 1992. The apparatus was a more sophisticated version of early EMBL devices with a controlled environment developed in Haifa by Talmon's group (Bellare et al, 1988), to which we added a time-resolved xenon flash unit that was kindly donated by Nigel Unwin.

plunge-freeze method for preparing a thin film of vitreous ice in which the biological structures of interest were suspended (Adrian et al, 1984; Dubochet et al, 1988). A photograph of their early apparatus is shown in Figure 6 and a collage explaining the principle is shown in Figure 7. This method, which consists of applying a drop of solution to an electron microscope grid, then blotting with filter paper for a few seconds to form a thin film, followed by plunging the grid into liquid ethane at liquid nitrogen temperature, is essentially the same method that most people still use 35 years later. The procedure together with many beautiful cryoEM images was explained in a comprehensive review (Dubochet et al, 1988).

EARLY SINGLE PARTICLE IMAGE ANALYSIS

Joachim Frank was the earliest to appreciate that structural information could be extracted from noisy electron microscope images of single particles (Frank, 1975; Frank & Al-Ali, 1975). With Marin van Heel, he introduced a powerful method, called multivariate statistical analysis, for extracting averages representing the typical, noise-free appearances of the different image subpopulations found in a stack of individual images (van Heel & Frank, 1981; Frank & van Heel, 1982). This early single particle work on classification of projection images of negatively stained biological structures became more powerful when the transition was made from 2D into 3D with the introduction of angular reconstitution by van Heel (1987) and the Random Conical Tilt (RCT) method by Radermacher et al. (1987). These methods allowed 3D structures to be obtained for the first time from single particle images of non-symmetrical structures. When these single particle methods were then applied to cryoEM images of specimens made using the Dubochet plunge-freeze method, the first single particle 3D structures of the ribosome were obtained (Frank et al, 1991), initially at low resolution, and then gradually improving (Gabashvili et al, 2000).

SINGLE PARTICLE CRYOEM – BLOBOLOGY IN THE EARLY DAYS

By the early 1980s, the steady progress in electron microscopy, electron cryomicrosopy, and calculation of 3D structures from EM images of all sorts of specimens led Wah Chiu and Nigel Unwin to propose a new Gordon Research Conference (GRC) theme, which they called "Three-dimensional electron microscopy of macromolecules", abbreviated to 3DEM. The first conference photograph is shown in Figure 8, with Nigel and Wah in the front row, surrounded by many others already mentioned above. The topic was timely and the 3DEM GRC has grown in size and frequency over the years.

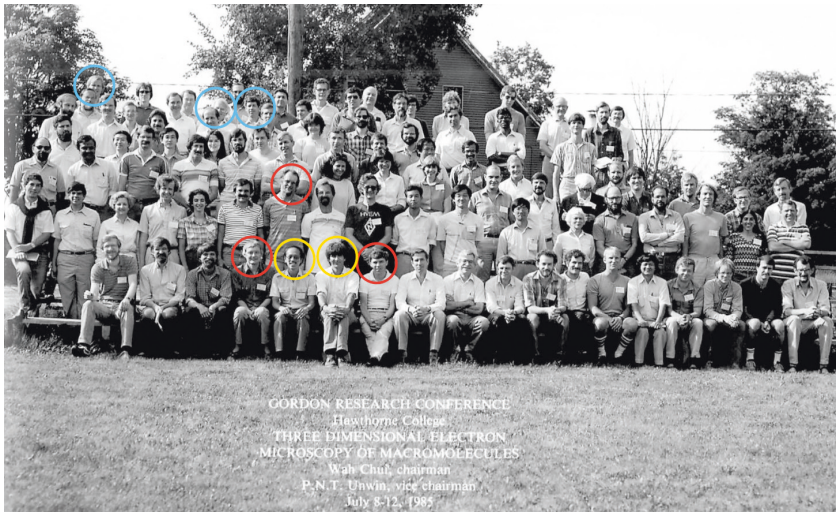

Figure 8. Group photograph from the first Gordon Research Conference on "Three Dimensional Electron Microscopy of Macromolecules" in 1985, with Wah Chiu and Nigel Unwin as chairman and vice chairman, circled in yellow. Also shown, circled in red are the three 2017 Chemistry Nobel laureates sitting or standing as close as possible to the organisers. In the back row, circled in blue are Bob Glaeser, Ken Taylor and Ken Downing, who also had key roles in the early development of cryoEM.

Around 1987, the X-ray crystallographers had also started to explore freezing 3D crystals to liquid nitrogen temperature, which had been applied already to crystals of small organic molecules (Hope & Nichols, 1981). Håkon Hope spent a year working with Ada Yonath's group and managed to obtain much better diffraction patterns of ribosome 3D crystals than could be obtained without freezing (Hope et al, 1989). At that time, the intensity of X-ray sources at synchrotrons was not sufficient to observe any fading of the diffraction patterns from frozen crystals due to X-ray radiation damage but it was clear from a comparison of the amount of energy deposited by electron and X-ray irradiation that this was simply due to the relatively weak X-ray beams available then (Henderson, 1990). As a consequence of my interest in the importance of radiation damage in electron microscopy, I was invited to give a talk at a meeting in Grenoble to discuss the possibility of building an X-ray microscopy beam line at the planned European Synchroton Radiation Facility (ESRF). To my surprise, many of those present did not know about the mechanisms and consequences of radiation damage, so I decided to write a review comparing radiation damage by electrons with that from X-rays. While I was writing the review, a copy of "Neutron News" arrived with a centre-page pull-out supplement listing the nuclear reactions and cross-sections for the interaction of neutrons with all the isotopes of all the elements (Sears, 1992). This allowed a calculation of the ratio of elastic to inelastic cross-sections

and the resulting energy deposited during neutron illumination to be added to the review. The result was a broad review describing the potential and limitations of neutrons, electrons and X-rays for high-resolution imaging of biological macromolecules. The conclusion was that electrons produced the least damage per useful elastically scattered event, by a factor of 3 less than neutrons and a factor of 1000 less than X-rays. The review went on to estimate the minimum molecular weight of a macromolecular assembly and the approximate number of single particle images that would be required to determine the atomic structure by single particle cryoEM without resorting to crystallisation either in 2D or 3D (Henderson, 1995).

Since by then it was also becoming clear that it was just as difficult to make well-ordered 2D crystals as it was to make well-ordered 3D crystals of membrane proteins, I decided to switch the efforts of our group from electron crystallography to single particle cryoEM. This brought with it a number of new requirements. Since all of the information, both amplitudes and phases, would now come from the images, the electron diffraction patterns could no longer compensate for poor quality images. The microscopes would need more stable stages, better vacuums and the much brighter sources that were provided by field emission electron guns. Consequently, at MRC-LMB we purchased a Hitachi HF-2000 and this was used by Bettina Böttcher in Tony Crowther's group to obtain the first single particle structure with sub-nanometre resolution. The structure of the icosahedral assembly of hepatitis B core protein reached 7.4 Å resolution (Böttcher et al, 1997), and revealed the presence of a bundle of 4 α-helices protruding from the surface, which could be interpreted in terms of the amino acid sequence. Bettina used over 6000 particles in her work, which was still several orders of magnitude greater than the theory (Henderson, 1995) suggested and had a B-factor of about 500 $Å^2$. The B-factor, also called temperature factor or Debye-Waller factor, is an excellent way to describe how the power in Fourier components fades with resolution. The very high B-factor of 500 $Å^2$ in this case realistically ruled out being able to go to higher resolution without understanding the origin of the loss of contrast that limited the resolution. Many other structures of icosahedral viruses and helically ordered assemblies had been studied by cryoEM, but few reached 10 Å resolution by then. This was the era when cryoEM was termed "blobology" because the resolution of all the maps, except those from 2D crystals, merely revealed blobs of density for individual protein domains, which was insufficient to resolve the path of the polypeptide or the chemistry of the amino acids. A summary of the historical progress of cryoEM for HepB is shown in Figure 9: atomic resolution was not reached until 2013 when Hong Zhou's group reached 3.5 Å by collecting thousands of images on film. A summary of the

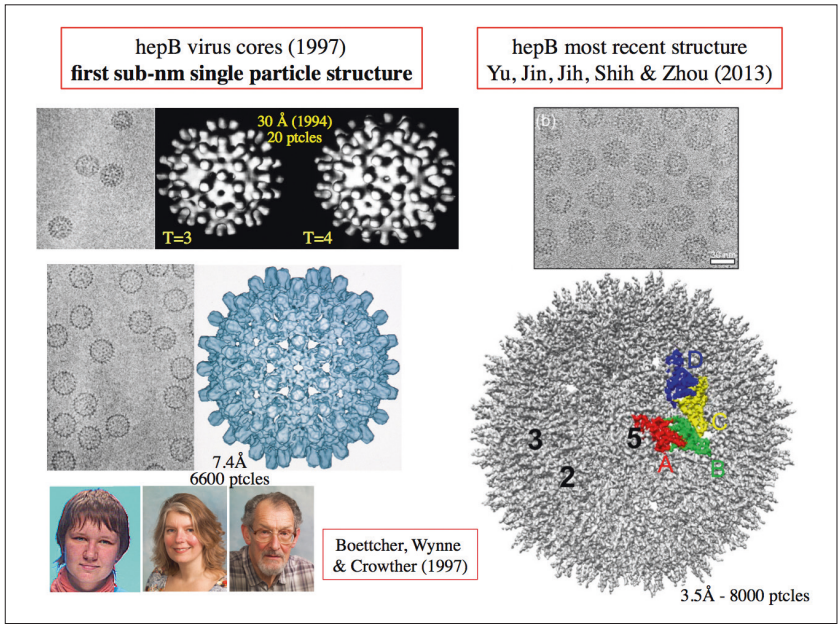

Figure 9. Three stages in the progress of cryoEM studies of the hepatitis B virus cores. The top left panel shows the first cryoEM 3D maps at 30 Å resolution obtained in 1994 from samples brought by Nikolai Kiselev from Paul Pumpens in Riga, Latvia. The sample had a mixture of T=3 and T=4 particles, but both 3D maps show similar protrusions, from Crowther et al (1994). The bottom left panels show a cryoEM image and 7.4 Å structure from the work of Böttcher et al (1997), which was the first sub-nm single particle cryoEM structure. It was calculated using ~6400 images of T=4 particles from an improved preparation. It showed that each protrusion consisted of a bundle of 4 α-helices. Finally, the panels on the right show a more recent cryoEM image and the 3.5Å resolution 3D structure from the work of Yu et al. (2013) in which they used many more images on a better microscope, but still using film as the recording medium. Similar resolutions can now be obtained using the new detectors with substantially fewer particles.

state-of-the-art of cryoEM in 2001 is shown in Figure 10, which includes a panel showing the structure of the *E. coli* 70S ribosome at 11.5 Å resolution (Gabashvili et al, 2000).

Niko Grigorieff had joined our group initially to work on the refinement of the bacteriorhodopsin structure. After completing this work (Grigorieff & Henderson, 1995; 1996; Grigorieff et al. 1995; 1996), he wrote a new single particle program called Frealign, which he used to determine at 22 Å resolution the first cryoEM structure of mitochondrial Complex I (Grigorieff, 1998), chosen to be an interesting structure without any internal symmetry. Grigorieff wrote Frealign specifically to treat all the electron optical parameters, such as defocus and astigmatism that were required for high-resolution single particle cryoEM, with the aim of being complementary to earlier 3DEM program suites such as Imagic (van Heel et al, 1996) and Spider (Frank et al, 1996).

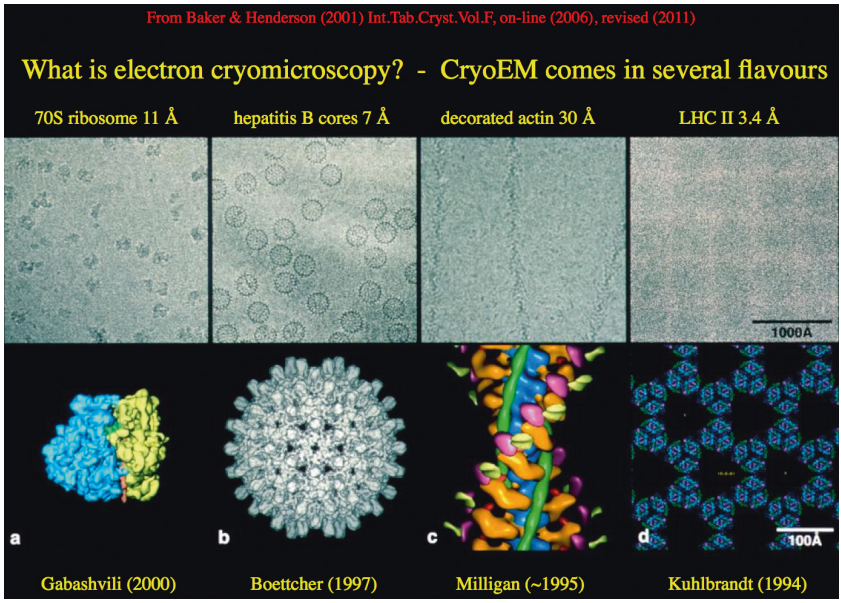

Figure 10. Reproduced from Baker & Henderson, 2001; 2012. Examples of macromolecules studied by cryoEM and 3D image reconstruction and the resulting 3D structures (bottom row) after cryoEM analysis dating from around the year 2000. All micrographs (top row) are displayed at ~170,000x magnification and all models at ~1,200,000x magnification. (a) A single particle without symmetry. The micrograph shows 70S E. coli ribosomes complexed with mRNA and fMet-tRNA. The surface-shaded density map, made by averaging 73,000 ribosome images from 287 micrographs, has a resolution of 11.5 Å. The 50S and 30S subunits and the tRNA are coloured blue, yellow and green, respectively. The identity of many of the protein and RNA components were known and some RNA double helices were clearly recognisable by their major and minor grooves (e.g. helix 44 is shown in red). Courtesy of J. Frank, using data from Gabashvili et al. (2000). (b) A single particle with symmetry. The micrograph shows hepatitis B virus cores. The 3D reconstruction, at a resolution of 7.4 Å, was computed from ~6400 particle images taken from 34 micrographs. From Böttcher et al (1997). (c) A helical filament. The micrograph shows actin filaments decorated with myosin S1 heads containing the essential light chain. The 3D reconstruction, at a resolution of 30–35 Å, is a composite in which the differently coloured parts are derived from a series of difference maps that were superimposed on F-actin. The components include: F-actin (blue), myosin heavy-chain motor domain (orange), essential light chain (purple), regulatory light chain (yellow), tropomyosin (green) and myosin motor domain N-terminal beta-barrel (magenta). Courtesy of A. Lin, M. Whittaker & R. Milligan (Scripps Research Institute, La Jolla). (d) A 2D crystal: light-harvesting complex LHCII at 3.4 Å resolution (Kühlbrandt et al, 1994). The model shows the protein backbone and the arrangement of chromophores in a number of trimeric subunits in the crystal lattice. In this example, image contrast is too low to see any hint of the structure without image processing. Courtesy of W. Kühlbrandt (Max-Planck-Institute for Biophysics, Frankfurt).

At around this time, Peter Rosenthal joined our group and recorded single particle cryoEM images of several interesting structures (e.g. Rosenthal et al, 2003). Sriram Subramaniam and Jacqueline Milne had also arrived on a sabbatical visit that for a variety of reasons was extended to 3 years. Jacqueline calculated a 3D structure of the pyruvate dehydrogenase complex (Milne et al, 2002) from images of single particles embedded in amorphous ice, using Marin van Heel's Imagic package (van Heel et al, 1996) to get started and Niko Grigorieff's Frealign (Grigorieff, 1998) for higher resolution refinement, with samples supplied by Gonzalo Domingo in Richard Perham's group in the Biochemistry Department.

An initial project by Peter Rosenthal to develop a semi-automatic procedure for determination of the absolute hand of a single particle cryoEM structure by using tilt pair images developed into a much broader publication (Rosenthal & Henderson, 2003), which allowed us to propose a theoretical framework to describe and understand the results of single particle cryoEM studies, and to propose the "tilt-pair validation procedure". The tools he developed helped to explain why the resolution was limited in 3D cryoEM studies at that time and to suggest what would be needed to do better. The basic idea was that the predicted resolution-dependence of the electron scattering, at resolutions beyond about 10 Å, could be described by four factors – the electron-scattering form-factors for individual-atoms, Wilson statistics, image blurring and errors in the determination of the orientation parameters of the particles in the analysis. To a first approximation, a single B-factor could explain the observations both in theory and for a set of experimental data that consisted of 3600 single particle images of pyruvate dehydrogenase, with a B-factor of ~1000 $Å^2$. This high B-factor limited the resolution to 8.7 Å. Rosenthal also introduced a novel plot of the natural logarithm of the number of particles required to achieve different resolutions versus the reciprocal of resolution squared. In a light-hearted way, we referred to this as a universal resolution calculator, or "Rosenthal plot". It showed graphically that the most important factor to achieving higher resolution single particle cryoEM structures was to acquire better images in which the higher resolution Fourier components were recorded with less blurring and therefore less contrast loss. Better images would have lower intrinsic B-factors and would allow more accurate orientation determination leading to lower computational blurring, and lower overall B-factors. This image quality problem was essentially the same problem that had been identified in earlier publications (Henderson & Glaeser, 1985; Henderson, 1992), and provided the rationale for increased efforts to develop better electron detectors.

DEVELOPMENT OF DIRECT ELECTRON DETECTORS, IMPACT ON SINGLE PARTICLE CRYOEM, AND THE "RESOLUTION REVOLUTION"

During the 1990s, Wasi Faruqi who had worked earlier on the development of X-ray detectors with Hugh Huxley at MRC-LMB, switched his emphasis to the development of better detectors for electrons. Before that and in practice right up until 2012, photographic film had been the best medium for recording electron images, but suffered from the fact that the images were not immediately available since the film had to be developed, fixed, washed, dried and digitised on a film scanner. In addition, the emulsions had to be desiccated for weeks before use, otherwise the microscope vacuum would be compromised and the residual water vapour in the column would rapidly build up as a contaminating layer of ice on the cryo-specimens. After various projects to develop electron detectors based on phosphor/fibre-optics/CCD (Faruqi et al, 1995; 1999) or on the Medipix series of hybrid pixel detectors (Faruqi et al, 2003; 2005), Wasi identified work by Renato Turchetta at the Rutherford Appleton Laboratory (RAL) near Oxford on monolithic active pixel sensors (MAPS) using CMOS (complementary metal oxide semiconductor) technology. Turchetta had been investigating the use of these detectors for charged particle detection (Caccia et al, 1999) and had brought the Startracker CMOS detector to MRC-LMB in 2002. Tests immediately showed excellent sig-

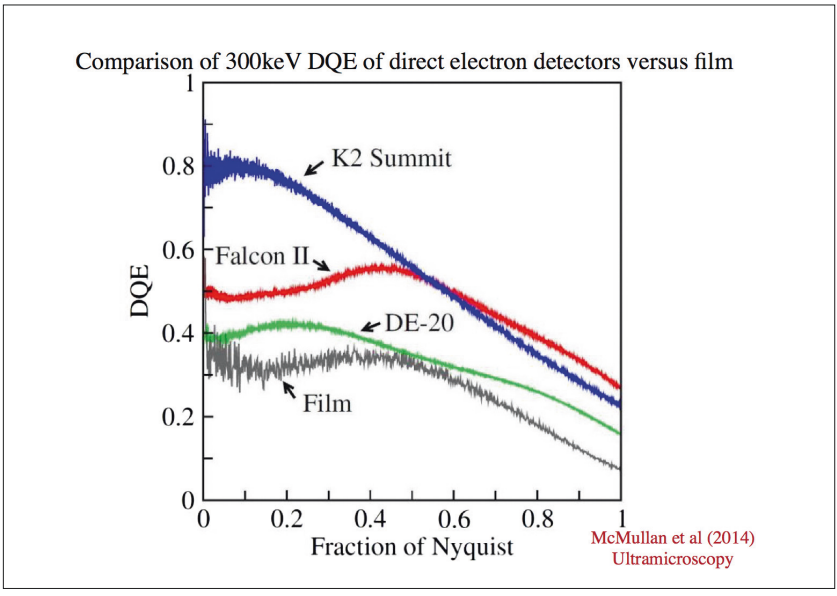

Figure 11. Comparison of performance of three direct electron detectors, reproduced from McMullan et al (2014). The DQE is measured as a function of spatial frequency for the DE-20 (green), Falcon-II (red) and K2 Summit (blue). The corresponding DQE of photographic film is shown in black.

nal-to-noise ratio for detection of 120 keV electrons, but also showed that the electron beam rapidly damaged the pixels. A long project to improve the radiation hardness and to optimise the detective quantum efficiency (DQE) then ensued, until publications in 2009 (McMullan et al, 2009a; 2009b; 2009c) showed that this type of direct detection device (DDD) would exceed the performance of film when used for imaging of high energy electrons (preferably 300 keV or higher), provided the sensors were backthinned.

The work with the RAL group eventually led to the commercial development of the Falcon detectors by FEI, now Thermo Fisher Scientific. In parallel, work by Gatan to develop the K2 CMOS detector, based on earlier work by Peter Denes, and by Direct Electron to develop the DE-12 detector, based on earlier work by Kleinfelder, Xuong and Ellisman, both produced similar CMOS cameras. A comparison of these three detectors with film is shown in Figure 11. All three had improved detective quantum efficiency (DQE) compared with film, but only the K2 detector at that time had fast enough read-out to allow implementation of an electron counting mode in which the analogue images were processed to replace the stochastic signal from individual electron events with an equal signal that represented the true nature of the image, and which gave the K2 a

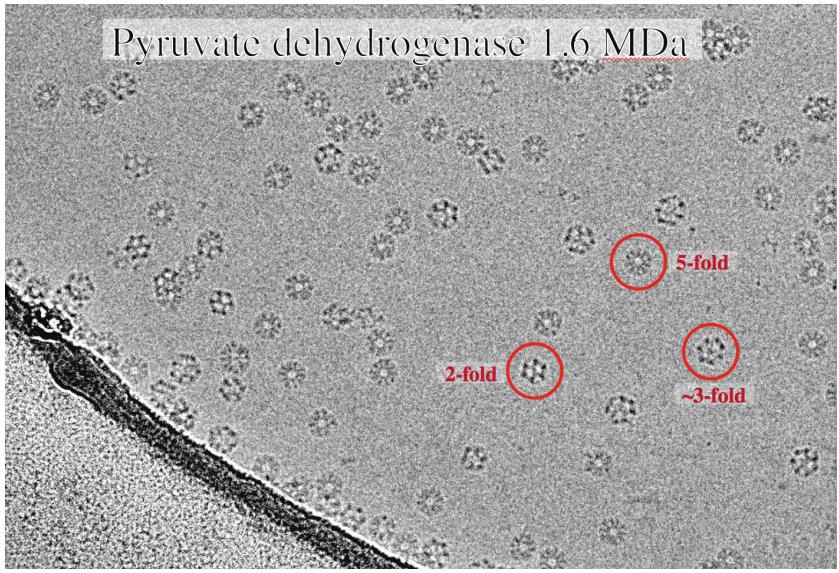

Figure 12. An example of a state-of-the-art cryoEM image with excellent signal-to-noise ratio. It shows each macromolecule very clearly with obvious orientations. This specimen was plunge-frozen by Peter Rosenthal in 2001 using a sample of pyruvate dehydrogenase from Richard Perham's group. The image was recorded in 2015 by Vinothkumar on a Falcon-II detector in integrating mode. The specimen, kept under liquid nitrogen for 14 years, still has perfectly amorphous ice.

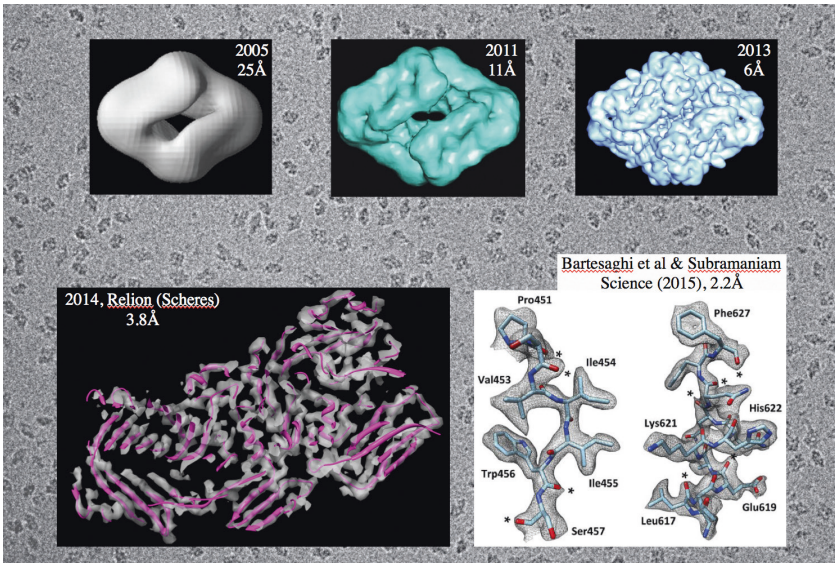

Figure 13. Progress of work on *E. coli* β-galactosidase, which was selected as a challenging test object in 1997. The underlying image shows a field of view recorded in 2013 on one of the direct electron detectors. The five superimposed panels show how technical progress has greatly improved the resolution during the last 20 years. The top left panel shows an attempt to obtain a low-resolution 3D structure from the earliest images recorded on film: we did not believe this structure even though it is roughly right. The top centre panel shows a medium resolution structure using images recorded on photographic film with 80 keV electrons. This was the first structure we proved was correct because it passed the tilt-pair validation test (Rosenthal & Henderson, 2003; Henderson et al, 2011). The top right structure was obtained using a direct electron detector that first became available in 2013 and immediately showed higher resolution. The use of Relion (bottom left) improved the resolution further to 3.8 Å. Finally, the work of Bartesaghi et al (2015), using higher magnification, produced a superb map at 2.2 Å resolution.

higher DQE at low resolution. In addition, the rolling shutter read-out mode for these CMOS sensors allowed the recording of the images as dose-fractionated exposure series, or "movies", which allowed subsequent computer-based correction for beam-induced specimen motion to be carried out (Brilot et al, 2012; Campbell et al, 2012; Bai et al, 2013; Li et al, 2013; Scheres, 2014; Vinothkumar et al, 2014a; Rubinstein & Brubaker, 2015; Grant & Grigorieff, 2015). The combination of increased DQE and specimen motion correction greatly improved the quality of the images, and this alongside the development of improved computer image processing algorithms such as in Relion (Scheres, 2012) resulted in a quantum leap in the resolution of single particle cryoEM structures (e.g. Liao et al, 2013; Amunts et al, 2014; Allegretti et al, 2014). This advance was characterised by the term "Resolution Revolution" (Kühlbrandt, 2014) and has proved to be an apt description. An example of the clarity seen in these new images is shown in Figure 12.

There have been many superb structures determined by single particle cryoEM at near-atomic resolution during the last 5 years; I briefly mention three with which I had an early involvement, and which were subsequently pursued to higher resolution by younger colleagues. Two of these are shown in Figure 13 and Figure 14. The first (Figure 13) is β-galactosidase from *E. coli*, which had reached a resolution of only 11 Å when images had been recorded at 80 keV on film (Henderson et al, 2011), but rapidly went to 6 Å (Vinothkumar et al, 2014a), then 3.8 Å using Relion, and finally 2.2 Å through the work of Bartesaghi et al (2015), when higher quality images recorded with the new DDD cameras were obtained. The second structure (Figure 14) is that of mitochondrial Complex I from the work of Judy Hirst's group first at 5 Å resolution (Vinothkumar et al, 2014b) and then at 4.2 Å (Zhu et al, 2016), which allowed them to identify and build atomic models of all 45 polypeptides that make up the structure of this large macromolecular complex. Finally, the work of John Rubinstein on F_1F_o-ATPases also shows the impact of the resolution revolution on a structure that was only barely tractable 15 years ago – the 30 Å resolution obtained in 2003 (Rubinstein et al, 2003) has recently reached 3.7 Å (Zhou et al, 2015; Guo et al, 2017).

OUTSTANDING PROBLEMS

Two kinds of analysis are very revealing when applied to current cryoEM structural determinations. One of these is the Rosenthal plot, the slope of which can reveal the underlying B-factor that describes the behaviour of the data and limits the resolution of the final density map, in a robust way that does not require estimation of the modulation transfer function (MTF) of the detector. The best recent single particle cryoEM structure determinations show B-factors of 90–100 $Å^2$, which is an enormous improvement over the values of 500–1000 $Å^2$ that were obtained a decade earlier (Böttcher et al, 1997; Rosenthal & Henderson, 2003; Rubinstein et al, 2003). The other useful plot shows the information content against the frame number or electron dose from dose-fractionated "movies", as shown in Figure 15, reproduced from Henderson (2015). This second type of plot shows that the first few frames of the movies, which should have the least radiation damage, are actually much worse than those with exposures in the range 5–10 el/$Å^2$. They have less information, characterised by higher B-factors than later frames. These two diagnostic tools show that the images being acquired using present state-of-the-art approaches still fall significantly short of what would be expected in perfect images limited only by radiation damage and no other factor. The first frame of such a perfect image should show the highest contrast and the lowest B-factor, with a gradual increase in disorder in subsequent frames

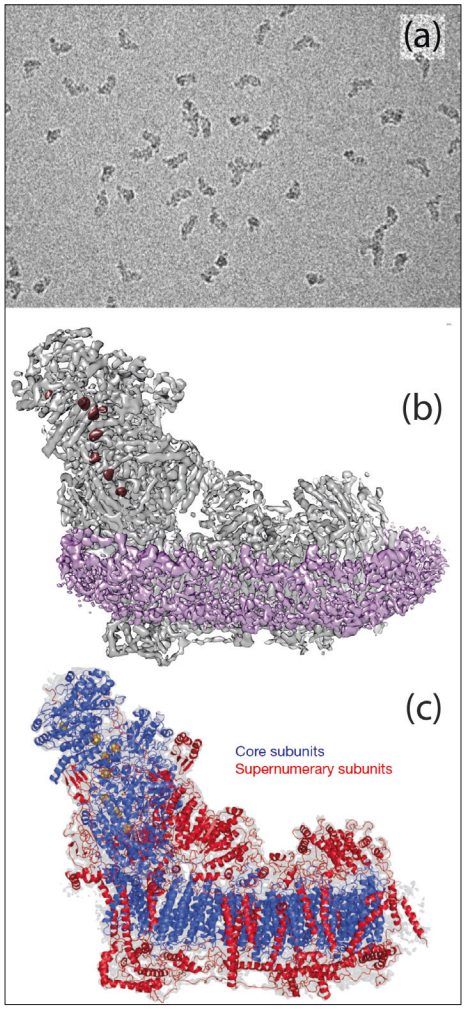

Figure 14. Mitochondrial Complex I. (a) cryoEM image. (b) 3D density map at three contour levels. (c) 3D model showing all 45 protein subunits. From Vinothkumar et al (2014b) and Zhu et al, (2016).

as radiation damage causes slightly different changes in the structure of the different molecules in the dataset. In addition, it is well-known that radiation damage causes mass loss due to the release of volatile radiation products (Müller & Engel, 2001). The dose-dependence of the intercept (C_f) parameter in the particle polishing procedure of Relion (Scheres, 2014) invariably shows a reduction of ~20% during the exposure, which is believed to be due to mass loss. To help understand the origin of the phenomena seen in these two types of plot, some recent publications allow the relative importance of several possible contributory factors to be estimated.

At liquid nitrogen temperature, hydrogen and oxygen are lost from both surfaces of the thin film of ice during electron irradiation, but the conse-

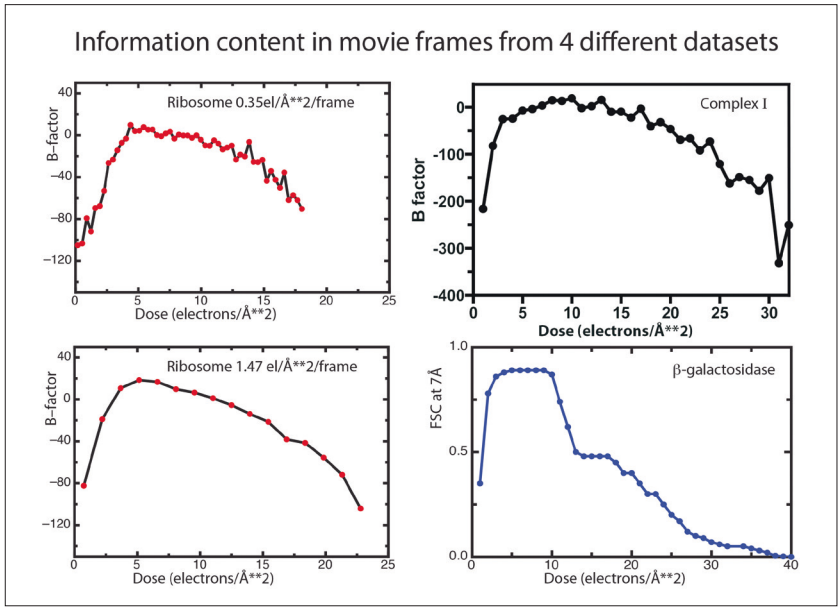

Figure 15. Plot of the B-factors or signal at 7 Å resolution in typical movie sequences, reproduced from Henderson (2015) with permission.

quence of radiolysis deeper inside the specimen simply consists of recombined water molecules whose positions have moved. McMullan et al (2015) showed that the water molecules in pure amorphous ice move during electron irradiation by about 1 Å after an electron dose of 1 el/Å^2 using 300 keV electrons. After a typical exposure of 25 el/Å^2, the average water molecule has therefore moved by ~5 Å. This pseudo-Brownian motion of the water molecules pushes around the embedded macromolecular assemblies being studied, but fortunately this causes only a small movement of the macromolecule, such as 0.5 Å for a ribosome and slightly more for smaller structures (McMullan et al, 2015). The resulting blurring of the images adds a small uniform B-factor to summed images but cannot explain the poor contrast and high B-factor in the first frames of the movies.

Recent work by Russo and Henderson has also allowed the impact of charge build-up during irradiation due to the "Berriman effect" (Brink et al, 1998), and of charge fluctuations in the thin layers of amorphous, non-conductive ice, often termed the "beeswarm effect", to be estimated. Both of these were measured to be finite but small. The Berriman effect was found to have an impact only during the very earliest part of the first frame of an exposure series and reached an equilibrium during the rest of the exposure (Russo & Henderson, 2018a). The beeswarm effect also produces a measurable perturbation in the images, which is manifested as a

small decrease in the amplitude of the envelope function that is detectable only at very high defocus values, well outside the range normally used for single particle cryoEM images (Russo & Henderson, 2018b).

The clear conclusion is that physical (i.e. mechanical) motion is the principal remaining factor that is causing the quality of the best current images to fall short of that expected in theory, which should be limited only by statistical disorder due to radiation damage. There are two possible causes of this physical motion and resultant image blurring. One is the beam-induced relaxation of stresses frozen into the specimen at the point of plunge-freezing, due to the different linear coefficients of expansion of protein (positive, since proteins shrink on freezing) and water (negative, since it expands on freezing), as well as the support, which constrains both. The second is a consequence of covalent bond breakage after radiation damage to the protein or nucleic acid in the macromolecular assembly. Bond breakage causes covalent bonds of length ~1.5 Å to increase to ~3.5 Å producing radiolytic fragments that are separated by van der Waals distances. Depending on their size, these radiolytic fragments will then be either trapped causing an increase in internal pressure or will diffuse away and evaporate creating a cavity and a decrease in internal pressure. Unless the contributions of trapped and released radiolytic fragments are exactly balanced, this will cause beam-induced local specimen motion, with resulting image blurring, of just the kind observed. We could say that we have a diagnosis but not a cure for the outstanding problem of beam-induced image blurring.

FUTURE

What will be the consequence of successfully eliminating or ameliorating the remaining problems of specimen motion and image blurring? Such an advance might be achieved as a consequence of improvements in specimen supports (e.g. Russo & Passmore, 2014), or of improvements in imaging protocols (e.g. Berriman & Rosenthal, 2012), or of improvements in computer-based motion correction of the dose-fractionated movies (e.g. Zheng et al, 2017). We do not yet have an accurate estimate of the slope of the intrinsic increase in disorder as a function of radiation dose, which is also likely to depend to some extent on the composition of the specimen. For example, it is known (Glaeser, 1971) that nucleic acid bases are on average more radiation resistant than amino acids, due to conjugation in the ring structures of the bases, and that the aromatic side chains of phenylalanine, tyrosine and tryptophan are more radiation resistant than other amino acids. However, if we estimate that the disorder in average protein structures increases by a B-factor equivalent of 6 $Å^2$ for each additional exposure to a dose of 1 el/$Å^2$ using 300 keV electrons, then the slope of the plot of information content versus electron exposure will

look similar to the asymptotic tail at higher doses in the plots of Figure 15. After 25 el/Å^2, the B-factor of that frame would then be 150 Å^2, and the average B-factor over the first 10 el/Å^2 of a dose-fractionated movie would be 30 Å^2. The resulting overall decrease from the current state-of-the-art B-factor (B_o) in single particle cryoEM of about 90 Å^2 about 30 Å^2 (B_n) would translate into a 30-fold reduction in the number of images required to reach 3 Å resolution [*viz.* $\exp((B_o - B_n)/2d^2)$], or alternatively an increase in resolution from 3.0 Å to ~1.7 Å [*viz.* $\sim d(B_n/B_o)^{1/2}$], or the ability to resolve an increased number of multiple states by 3D classification (Scheres et al, 2007) using the same number of images. It is safe to conclude that single particle cryoEM has a promising future.

ACKNOWLEDGEMENTS

Figure 16 shows a gallery of those who have contributed to the work described in this article. I am grateful to them all for being such wonderful collaborators and colleagues.

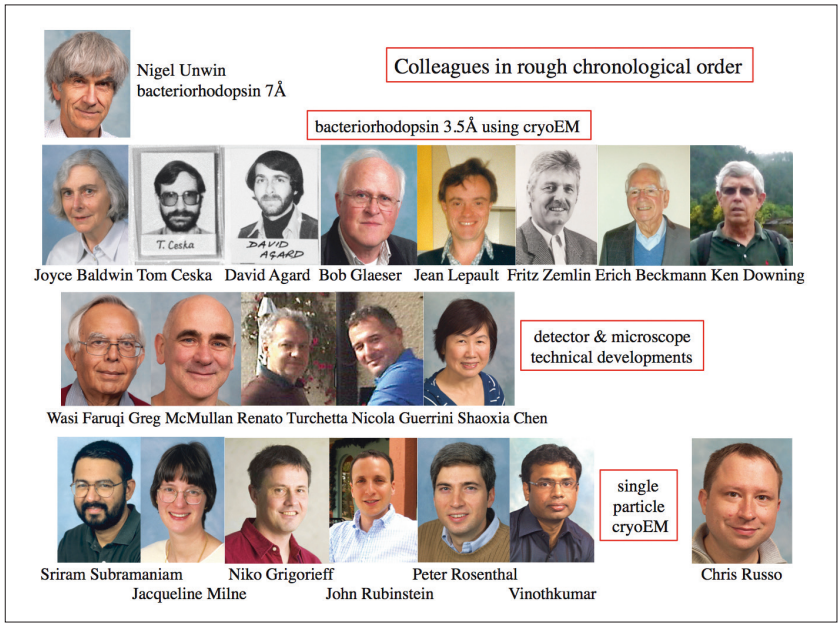

Figure 16. Colleagues who have contributed to the work described in this lecture. Top: Nigel Unwin. Second row: Joyce, Baldwin, Tom Ceska, David Agard, Jean Lepault, Fritz Zemlin, Erich Beckmann, Bob Glaeser, Ken Downing. Third row: Wasi Faruqi, Greg McMullan, Renato Turchetta, Nicola Guerrini, Shaoxia Chen. Bottom: Sriram Subramaniam, Jacqueline Milne, Niko Grigorieff, John Rubinstein, Peter Rosenthal, Kutti Ragunath Vinothkumar, Chris Russo.

REFERENCES

Adrian, M., Dubochet, J., Lepault, J. & McDowall, A. W. (1984). *Nature* **308**, 32–36.
Allegretti, M., Mills, D. J., McMullan, G., Kühlbrandt, W. & Vonck, J. (2014) *eLife*.01963.
Amunts, A., Brown, A., Bai, X.-C., Llacer, J. L., Hussain, T., Emsley, P., Long, F., Murshudov, G., Scheres, S. H. W. & Ramakrishnan, V. (2014) *Science* **343**, 1485–1489.
Bai, X.-C., Fernandez, I. S., McMullan, G. & Scheres, S. H. W. (2013). *eLife*.00461.
Baker, T. S. & Henderson, R. (2001). *In: International Tables for Crystallography, Vol. F, "Crystallography of Biological Macromolecules", Chapter 19.6 pp. 451–463; 473–479. (Ed. Rossmann, M.G. & Arnold, E.). Dordrecht: Kluwer Academic Publishers.*
Baker, T. S. & Henderson, R. (2012). *In: International Tables for Crystallography, Vol. F (second edition), "Crystallography of Biological Macromolecules", Chapter 19.6 pp. 593–614. (Ed. Rossmann, M.G. & Arnold, E.). Wiley.*
Bartesaghi, A., Merk, A., Banerjee, S., Matthies, D., Wu, X. W., Milne, J. L. S. & Subramaniam, S. (2015). *Science* **348**, 1147–1151.
Bellare, J. R., Davis, H. T., Scriven, L. E. & Talmon, Y. (1988). *J Electron Micr Tech* **10**, 87–111.
Berriman, J. A. & Rosenthal, P. B. (2012). *Ultramicroscopy* **116**, 106–114.
Blaurock, A. E. & Stoeckenius, W. (1971). *Nature-New Biol* **233**, 152–155.
Böttcher, B., Wynne, S. A. & Crowther, R. A. (1997). *Nature* **386**, 88–91.
Brilot, A. F., Chen, J. Z., Cheng, A. C., Pan, J. H., Harrison, S. C., Potter, C. S., Carragher, B., Henderson, R. & Grigorieff, N. (2012). *J Struct Biol* **177**, 630–637.
Brink, J., Sherman, M. B., Berriman, J. & Chiu, W. (1998). *Ultramicroscopy* **72**, 41–52.
Bullough, P. & Henderson, R. (1987). *Ultramicroscopy* **21**, 223–229.
Caccia, M., Campagnolo, R., Meroni, C., Kucewicz, W., Deptuch, G., Zalewska, A. & Turchetta, R. (1999). *arXiv*:hep-ex/ 9910019v1.
Campbell, M. G., Cheng, A. C., Brilot, A. F., Moeller, A., Lyumkis, D., Veesler, D., Pan, J. H., Harrison, S. C., Potter, C. S., Carragher, B. & Grigorieff, N. (2012). *Structure* **20**, 1823–1828.
Ceska, T. A. & Henderson, R. (1990). *J Mol Biol* **213**, 539–560.
Crowther, R. A., Kiselev, N. A., Böttcher, B., Berriman, J. A., Borisova, G. P., Ose, V. & Pumpens, P. (1994). *Cell* **77**, 943–950.
Downing, K. H. (1988). *Ultramicroscopy* **24**, 387–398.
Dubochet, J., Adrian, M., Chang, J. J., Homo, J. C., Lepault, J., McDowall, A. W. & Schultz, P. (1988). *Q Rev Biophys* **21**, 129–228.
Dubochet, J., Adrian, M., Teixeira, J., Alba, C. M., Kadiyala, R. K., Macfarlane, D. R. & Angell, C. A. (1984). *J Phys Chem* **88**, 6727–6732.
Dubochet, J., Chang, J. J., Freeman, R., Lepault, J. & McDowall, A. W. (1982a). *Ultramicroscopy* **10**, 55–61.
Dubochet, J., Lepault, J., Freeman, R., Berriman, J. A. & Homo, J. C. (1982b). J *Microsc* **128**, 219–237.
Faruqi, A. R., Andrews, H. N. & Henderson, R. (1995). *Nucl Instrum Meth* **A 367**, 408–412.
Faruqi, A. R., Cattermole, D. M., Henderson, R., Mikulec, B. & Raeburn, C. (2003). *Ultramicroscopy* **94**, 263–276.
Faruqi, A. R., Henderson, R., Pryddetch, M., Allport, P. & Evans, A. (2005). *Nucl Instrum Meth* **A 546**, 170–175.

Faruqi, A. R., Henderson, R. & Subramaniam, S. (1999). *Ultramicroscopy* **75**, 235–250.
Frank, J. (1975). *Ultramicroscopy* **1**, 159–162.
Frank, J. & Alali, L. (1975). *Nature* **256**, 376–379.
Frank, J., Penczek, P., Grassucci, R. & Srivastava, S. (1991). *J Cell Biol* **115**, 597–605.
Frank, J., Radermacher, M., Penczek, P., Zhu, J., Li, Y. H., Ladjadj, M. & Leith, A. (1996). *J Struct Biol* **116**, 190–199.
Frank, J. & vanHeel, M. (1982). *J Mol Biol* **161**, 134–137.
Gabashvili, I. S., Agrawal, R. K., Spahn, C. M. T., Grassucci, R. A., Svergun, D. I., Frank, J. & Penczek, P. (2000). *Cell* **100**, 537–549.
Glaeser, R. M. (1971). *J Ultrastruct Res* **36**, 466–482.
Grant, T. & Grigorieff, N. (2015). *eLife.*06980
Grigorieff, N. (1998). *J Mol Biol* **277**, 1033–1046.
Grigorieff, N., Beckmann, E. & Zemlin, F. (1995). *J Mol Biol* **254**, 404–415.
Grigorieff, N., Ceska, T. A., Downing, K. H., Baldwin, J. M. & Henderson, R. (1996). *J Mol Biol* **259**, 393–421.
Grigorieff, N. & Henderson, R. (1995). *Ultramicroscopy* **60**, 295–309.
Grigorieff, N. & Henderson, R. (1996). *Ultramicroscopy* **65**, 101–107.
Guo, H., Bueler, S. A. & Rubinstein, J. L. (2017). *Science* **358**, 936–940.
Hayward, S. B. & Stroud, R. M. (1981). *J Mol Biol* **151**, 491–517.
Henderson, R. (1970). *J Mol Biol* **54**, 341–354.
Henderson, R. (1990). *P Roy Soc B-Biol Sci* **241**, 6–8.
Henderson, R. (1992). *Ultramicroscopy* **46**, 1–18.
Henderson, R. (1995). *Q Rev Biophys* **28**, 171–193.
Henderson, R. (2015). *Arch Biochem Biophys* **581**, 19–24.
Henderson, R. & Baldwin, J. M. (1986). *44th Annu. Proc. EMSA* (Bailey, G. W., ed.), pp. 6– 9, San Francisco Press.
Henderson, R., Baldwin, J. M., Ceska, T. A., Zemlin, F., Beckmann, E. & Downing, K. H. (1990). *J Mol Biol* **213**, 899–929.
Henderson, R., Baldwin, J. M., Downing, K. H., Lepault, J. & Zemlin, F. (1986). *Ultramicroscopy* **19**, 147–178.
Henderson, R., Chen, S. X., Chen, J. Z., Grigorieff, N., Passmore, L. A., Ciccarelli, L., Rubinstein, J. L., Crowther, R. A., Stewart, P. L. & Rosenthal, P. B. (2011). *J Mol Biol* **413**, 1028–1046.
Henderson, R. & Glaeser, R. M. (1985). *Ultramicroscopy* **16**, 139–150.
Henderson, R., Raeburn, C. & Vigers, G. (1991). *Ultramicroscopy* **35**, 45–53.
Henderson, R. & Unwin, P. N. T. (1975). *Nature* **257**, 28–32.
Henderson, R. & Wang, J. H. (1972). *Biochemistry* **11**, 4565–4569.
Hope, H., Frolow, F., Vonbohlen, K., Makowski, I., Kratky, C., Halfon, Y., Danz, H., Webster, P., Bartels, K. S., Wittmann, H. G. & Yonath, A. (1989). *Acta Crystallogr* **B 45**, 190–199.
Hope, H. & Nichols, B. G. (1981). *Acta Crystallogr* **B 37**, 158–161.
Jeng, T. W., Chiu, W., Zemlin, F. & Zeitler, E. (1984). *J Mol Biol* **175**, 93–97.
Kimura, Y., Vassylyev, D. G., Miyazawa, A., Kidera, A., Matsushima, M., Mitsuoka, K., Murata, K., Hirai, T. & Fujiyoshi, Y. (1997). *Nature* **389**, 206–211.
Kühlbrandt, W. (2014). *Science* **343**, 1443–1444.
Kühlbrandt, W., Wang, D. N. & Fujiyoshi, Y. (1994). *Nature* **367**, 614–621.
Li, X. M., Mooney, P., Zheng, S., Booth, C. R., Braunfeld, M. B., Gubbens, S., Agard, D. A. & Cheng, Y. F. (2013). *Nat Methods* **10**, 584–590.
Liao, M. F., Cao, E. H., Julius, D. & Cheng, Y. F. (2013). *Nature* **504**, 107–112.

Lücke, H., Schobert, B., Richter, H. T., Cartailler, J. P. & Lanyi, J. K. (1999). *J Mol Biol* **291**, 899–911.
Matthews, B. W., Sigler, P. B., Henderson, R. & Blow, D. M. (1967). *Nature* **214**, 652–656.
McMullan, G., Chen, S., Henderson, R. & Faruqi, A. R. (2009a). *Ultramicroscopy* **109**, 1126–1143.
McMullan, G., Faruqi, A. R., Henderson, R., Guerrini, N., Turchetta, R., Jacobs, A. & van Hoften, G. (2009b). *Ultramicroscopy* **109**, 1144–1147.
McMullan, G., Clark, A. T., Turchetta, R. & Faruqi, A. R. (2009c). *Ultramicroscopy* **109**, 1411–1416.
McMullan, G., Faruqi, A. R., Clare, D. & Henderson, R. (2014). *Ultramicroscopy* **147**, 156–163.
McMullan, G., Vinothkumar, K. R. & Henderson, R. (2015). *Ultramicroscopy* **158**, 26–32.
Milne, J. L. S., Shi, D., Rosenthal, P. B., Sunshine, J. S., Domingo, G. J., Wu, X. W., Brooks, B. R., Perham, R. N., Henderson, R. & Subramaniam, S. (2002). *Embo J* **21**, 5587–5598.
Müller, S. A. & Engel, A. (2001). *Micron* **32**, 21–31.
Nogales, E., Wolf, S. G. & Downing, K. H. (1998). *Nature* **391**, 199–203.
Oesterhelt, D. & Stoeckenius, W. (1971). *Nature-New Biol* **233**, 149–152.
Pebay-Peyroula, E., Rummel, G., Rosenbusch, J. P. & Landau, E. M. (1997). *Science* **277**, 1676–1681.
Radermacher, M., Wagenknecht, T., Verschoor, A. & Frank, J. (1987). *J Microsc-Oxford* **146**, 113–136.
Rosenthal, P. B. & Henderson, R. (2003). *J Mol Biol* **333**, 721–745.
Rosenthal, P. B., Waddington, L. J. & Hudson, P. J. (2003). *J Mol Biol* **334**, 721–731.
Rossmann, M. G. & Henderson, R. (1982). *Acta Crystallogr* **A 38**, 13–20.
Rubinstein, J. L. & Brubaker, M. A. (2015). *J Struct Biol* **192**, 188–195.
Rubinstein, J. L., Walker, J. E. & Henderson, R. (2003). *Embo J* **22**, 6182–6192.
Russo, C. J. & Henderson, R. (2018a). *Ultramicroscopy* **187**, 43–49.
Russo, C. J. & Henderson, R. (2018b). *Ultramicroscopy* **187**, 56–63.
Russo, C. J. & Passmore, L. A. (2014). *Science* **346**, 1377–1380.
Scheres, S. H. W. (2012). *J Struct Biol* **180**, 519–530.
Scheres, S. H. W. (2014). *eLife*.03665
Scheres, S. H. W., Gao, H. X., Valle, M., Herman, G. T., Eggermont, P. P. B., Frank, J. & Carazo, J. M. (2007). *Nat Methods* **4**, 27–29.
Sears, V. F. (1992). *Neutron News* **3**(3), 26–37.
Smith, D. J., Saxton, W. O., O'Keefe, M. A., Wood, G. J. & Stobbs, W. M. (1983). *Ultramicroscopy* **11**, 263–281.
Steitz, T. A., Henderson, R. & Blow, D. M. (1969). *J Mol Biol* **46**, 337–348.
Subramaniam, S., Gerstein, M., Oesterhelt, D. & Henderson, R. (1993). *Embo J* **12**, 1–8.
Subramaniam, S. & Henderson, R. (2000). *Nature* **406**, 653–657.
Subramaniam, S., Lindahl, M., Bullough, P., Faruqi, A. R., Tittor, J., Oesterhelt, D., Brown, L., Lanyi, J. & Henderson, R. (1999). *J Mol Biol* **287**, 145–161.
Taylor, K. A. & Glaeser, R. M. (1974). *Science* **186**, 1036–1037.
Taylor, K. A. & Glaeser, R. M. (1976). *J Ultrastruct Res* **55**, 448–456.
Tsygannik, I. N. & Baldwin, J. M. (1987). *Eur Biophys J* **14**, 263–272.
Unwin, P. N. T. & Henderson, R. (1975). *J Mol Biol* **94**, 425–440.
van Heel, M. (1987). *Ultramicroscopy* **21**, 111–123.
van Heel, M. & Frank, J. (1981). *Ultramicroscopy* **6**, 187–194.

van Heel, M., Harauz, G., Orlova, E. V., Schmidt, R. & Schatz, M. (1996). *J Struct Biol* **116**, 17–24.
Vinothkumar, K. R., McMullan, G. & Henderson, R. (2014a). *Structure* **22**, 621–627.
Vinothkumar, K. R., Zhu, J. P. & Hirst, J. (2014b). *Nature* **515**, 80–84.
Yu, X. K., Jin, L., Jih, J., Shih, C. H. & Zhou, Z. H. (2013). *Plos One* 0069729.
Zemlin, F. (1979). *Ultramicroscopy* **4,** 241–245.
Zheng, S. Q., Palovcak, E., Armache, J.-P., Verba, K. A., Cheng, Y. & Agard, D. A. (2017) *Nat Methods* **14**, 331–332.
Zhou, A. N., Rohou, A., Schep, D. G., Bason, J. V., Montgomery, M. G., Walker, J. E., Grigorieff, N. & Rubinstein, J. L. (2015). *eLife*.10180.
Zhu, J. P., Vinothkumar, K. R. & Hirst, J. (2016). *Nature* **536**, 354–360.